

© MICROSCOPY SOCIETY OF AMERICA 2016

Microwave Frequency Comb from a Semiconductor in a Scanning Tunneling Microscope

Mark J. Hagmann, 1,2,* Dmitry A. Yarotski, and Marwan S. Mousa

Abstract: Quasi-periodic excitation of the tunneling junction in a scanning tunneling microscope, by a mode-locked ultrafast laser, superimposes a regular sequence of 15 fs pulses on the DC tunneling current. In the frequency domain, this is a frequency comb with harmonics at integer multiples of the laser pulse repetition frequency. With a gold sample the 200th harmonic at 14.85 GHz has a signal-to-noise ratio of 25 dB, and the power at each harmonic varies inversely with the square of the frequency. Now we report the first measurements with a semiconductor where the laser photon energy must be less than the bandgap energy of the semiconductor; the microwave frequency comb must be measured within $200 \,\mu\text{m}$ of the tunneling junction; and the microwave power is 25 dB below that with a metal sample and falls off more rapidly at the higher harmonics. Our results suggest that the measured attenuation of the microwave harmonics is sensitive to the semiconductor spreading resistance within 1 nm of the tunneling junction. This approach may enable sub-nanometer carrier profiling of semiconductors without requiring the diamond nanoprobes in scanning spreading resistance microscopy.

Key words: scanning tunneling microscopy, scanning probe microscopy, microwave frequency comb, spreading resistance, laser-assisted tunneling

Introduction

Yasui et al. (2011) generated microwave and terahertz frequency combs by mixing the radiation from two synchronized mode-locked ultrafast lasers in a photoconductive diode for frequency metrology. Mixing of two frequency combs generated in a high-speed photodetector with a single mode-locked laser has been employed in distance metrology (Doloca et al., 2010). In both applications the frequency combs are generated by optical rectification.

Since the 1960s, point-contact metal-insulator-metal diodes have been used for detection and mixing at frequencies up to 520 THz (Pollock et al., 1983), where detection is done through rectification in the tunneling junction. A review of laser-assisted scanning tunneling microscopy (STM) (Grafstrom, 2002) describes many studies of optical mixing and rectification in the tunneling junction of an STM.

In 2011, we generated the first microwave frequency comb (MFC) in an STM by focusing a mode-locked ultrafast laser on the tunneling junction using metal samples (Hagmann et al., 2011). Measurements with a spectrum analyzer showed that the linewidth is \sim 1 Hz (Hagmann et al., 2012*b*), but the apparent linewidth is a convolution of the actual power spectrum with the impulse response of the

Received May 31, 2016; accepted November 18, 2016 *Corresponding author. mhagmann@newpathresearch.com instrument, which was 1 Hz. Later measurements, using a resolution bandwidth of 0.1 Hz, showed a linewidth of ~0.1 Hz, which sets the present state-of-the-art for a narrow linewidth microwave source (Hagmann et al., 2013).

In tests with metal samples, there are hundreds of measurable harmonics and the power at each harmonic varies inversely with the square of the frequency. Analysis suggests that optical rectification causes the tunneling junction to act as a constant current source at each harmonic up to 30 THz, where the frequency is then one-half the reciprocal of the laser pulse width (15 fs) (Hagmann et al., 2013). Related phenomena are predicted in laser-assisted field emission (Hagmann & Mousa, 2007). Measurements show that current division between the shunting capacitance C_S at the tunneling junction and the load resistance R_L of the spectrum analyzer causes the power at the nth harmonic P_n as shown in the following equation:

$$P_n = P_1 \frac{1 + (2\pi R_L C_S f_1)^2}{1 + (2\pi R_L C_S n f_1)^2},\tag{1}$$

 f_1 , the fundamental frequency = the pulse repetition frequency of the laser. Typically, $C_S = 6.4 \,\mathrm{pF}$ and $R_L = 50 \,\Omega$, so the power in the second harmonic at 150.508 MHz is 94% of that at the fundamental frequency (75.254 MHz). At much higher frequencies the power at the nth harmonic varies inversely with the square of the frequency, corresponding to a decrease of 6 dB/octave.

¹Department of Electrical and Computer Engineering, University of Utah, Salt Lake City, UT 84112, USA

²NewPath Research LLC, Salt Lake City, UT 84115, USA

³Los Alamos National Laboratory, Center for Integrated Nanotechnologies, Materials Physics and Applications Division, Los Alamos, NM 87545, USA

⁴Department of Physics, Mu'tah University, Al-Karak 61710, Jordan

MATERIALS AND METHODS

In the recent measurements with semiconductors, we used a commercial STM (UHV-700; RHK Technology, Troy, Michigan) in air and ultrahigh vacuum. Freshly etched tungsten tips were annealed shortly before each measurement in vacuum, and freshly cut platinum–iridium tips were used for measurements in air. In some measurements, an external preamplifier (SR-570; Stanford Research Systems, Sunnyvale, California) coupled the tip to the STM control electronics, to increase the dynamic range of the DC tunneling current. A Kerr lens passively mode-locked Ti:Sapphire laser (CompactPro; Femtolasers, Wien, Austria) was focused to a $100-\mu m$ spot at the tunneling junction. The laser pulse length was 15 fs and the pulse repetition frequency was 74.254 MHz.

In these recent measurements we used an NI PXIe-5668R high-performance vector signal analyzer (VSA) and spectrum analyzer (National Instruments, Austin, Texas), interfaced to a computer with LabVIEW programming, to enable rapid acquisition and storage of the data. To allow rapid measurements in multiple files for statistical analysis, a resolution bandwidth of 2 Hz was used so the apparent linewidth in each scan was ~2 Hz. Each individual scan of 200 frequencies required an acquisition time of 590 ms.

A wide-bandgap semiconductor, n-GaN, was chosen to avoid creating electron-hole pairs with the laser, which can cause surge currents that interfere with the measurements (Hagmann et al., 2012a). The $3 \times 3 \times 0.5$ mm cut single crystal of intrinsic n-type semiconductor has a carrier concentration of $\sim 10^{16}/\text{m}^3$ and it was oriented for tunneling at the (0001) surface.

In the previous measurements with metal samples we used the apparatus shown in the block diagram in Figure 1. A bias-T, depicted as a capacitor and inductor, was inserted between the sample (dark circle) and the bias circuit of the STM, to permit connection to the spectrum analyzer.

However, in our measurements with semiconductors, the MFC was measured as shown in the block diagram in Figure 2, with a probe making contact with the semi-conductor within $200 \, \mu \mathrm{m}$ of the tunneling junction. Figure 3 shows why the MFC must be measured so close to the tunneling junction instead of using a bias-T.

The tunneling junction was forward biased to have sufficient DC tunneling current for the MFC to be measured. Each laser pulse causes a sub-nanometer spot of surface charge on the semiconductor and Figure 3 shows the processes for the dispersal of this charge with forward-biased

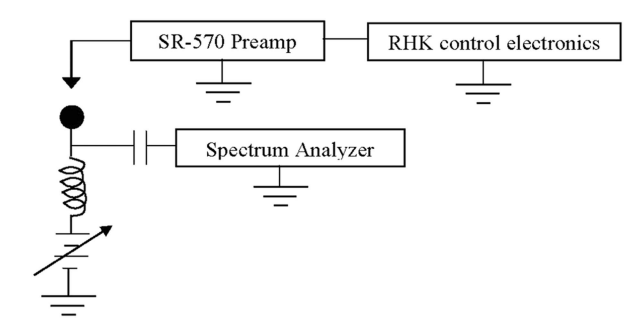


Figure 1. Block diagram for measurements with metal samples.

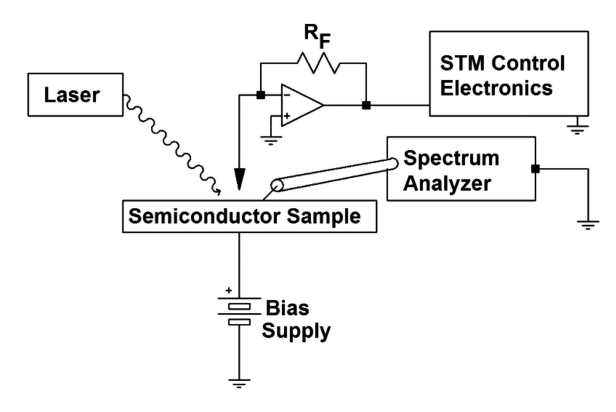


Figure 2. Block diagram for measurements with a semiconductor sample. STM, scanning tunneling microscope.

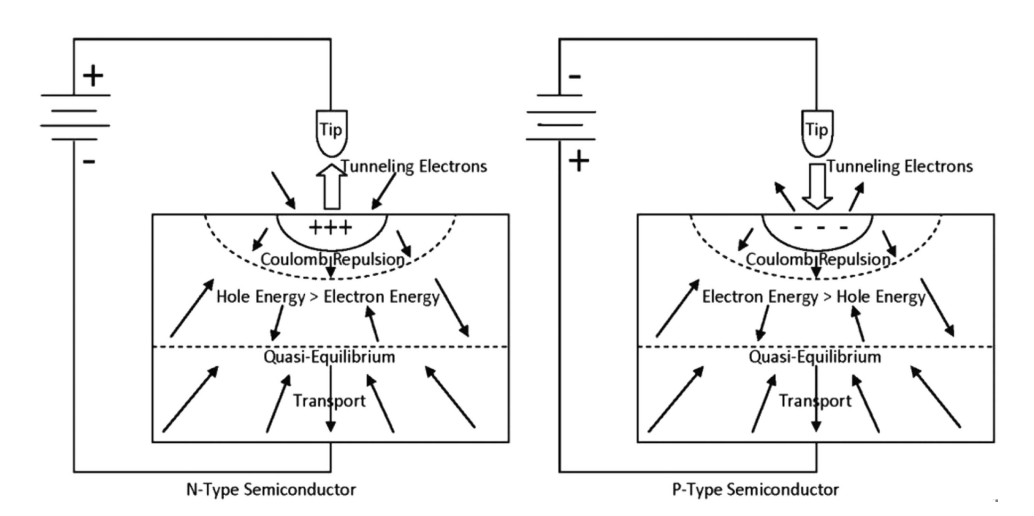


Figure 3. Processes for dispersal of the surface charge caused by a pulse of tunneling electrons in a forward-biased tunneling junction.

n-type and p-type semiconductors. The surface charge consists of ~400 minority carriers (Hagmann et al., 2015). Typically, dielectric relaxation takes place within 1 ps, which is 10^{-4} of the time between consecutive laser pulses; hence, the phenomena occurring in each pulse may be considered to be independent. The injected minority carriers move outward in a Coulomb explosion (Hagmann et al., 2015), as majority carriers move inward to complete neutralization in a distance of ~20 μ m. We find that the probe must be within $200 \, \mu$ m of the tunneling junction to detect the MFC, but ideally this distance should be <20 μ m.

Initially, the MFC was measured with a high-speed silicon PIN photodetector (DET 210; Thorlabs, Newton, New Jersey) in place of the tunneling junction. This was followed by measurements using the STM with a gold sample, to verify proper operation of the system, before beginning the measurements with the semiconductor.

We were concerned that optical rectification could take place at the contact between the probe and the semiconductor, so an ohmic contact to the semiconductor was formed, using an Al/Ti bilayer metallization (Lin et al., 1994). The bilayer consisted of a 5-nm thickness of titanium covered by a 100-nm layer of aluminum, where each layer had a common width of $100\,\mu\mathrm{m}$. However, this structure did not permit chemical cleaning of the semiconductor, which appears to be essential for the measurements. Our second approach, which was successful, was to clean the gallium nitride in HF and use a fine gold wire (8-mm long, 0.3-mm diameter) attached to the semiconductor with indium as a probe.

RESULTS AND DISCUSSION

Initial measurements of the MFC with the high-speed silicon PIN photodetector, as well as measurements with a gold sample in the STM, verified that the measurement system was operating properly. A series with 13 consecutive scans of the 18th harmonic (1.3366 GHz) with the photodetector showed an apparent linewidth (full-width at half-maximum) of 2.7 Hz with the peak power having a mean value of –119 dBm. A series of 286 consecutive scans of the 100th harmonic (7.4254 GHz) with a gold sample in the STM showed an apparent linewidth of 2.6 Hz with the peak power having a mean of –115 dBm. Using equation (1), this would be equivalent to a power of –92 dBm at the fundamental frequency, which is consistent with earlier tests.

The first measurements, using the semiconductor with the Al/Ti bilayer metallization for an ohmic contact, gave no detectable microwave power, which we attribute to the inability to clean the semiconductor at the tunneling junction. Following this, the gallium nitride was cleaned with HF and a fine gold wire (8-mm long, 0.3-mm diameter) was attached to the semiconductor with indium to serve as the probe, to enable the following measurements of the MFC.

Figures 4 to 7 show the average measured microwave power for 24 consecutive scans as a function of the frequency.

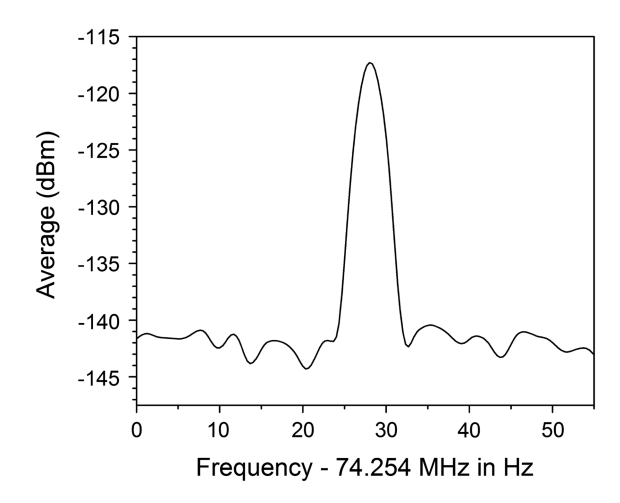


Figure 4. Mean power at the first harmonic of the microwave frequency comb for 24 consecutive scans with an n-type GaN sample in the scanning tunneling microscope.

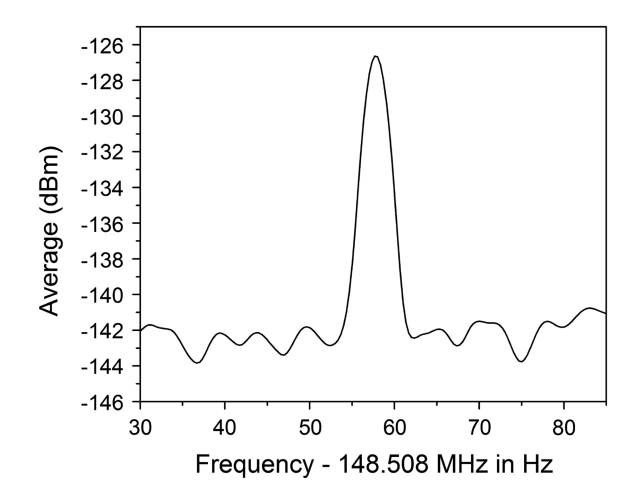


Figure 5. Mean power at the second harmonic of the microwave frequency comb for 24 consecutive scans with an n-type GaN sample in the scanning tunneling microscope.

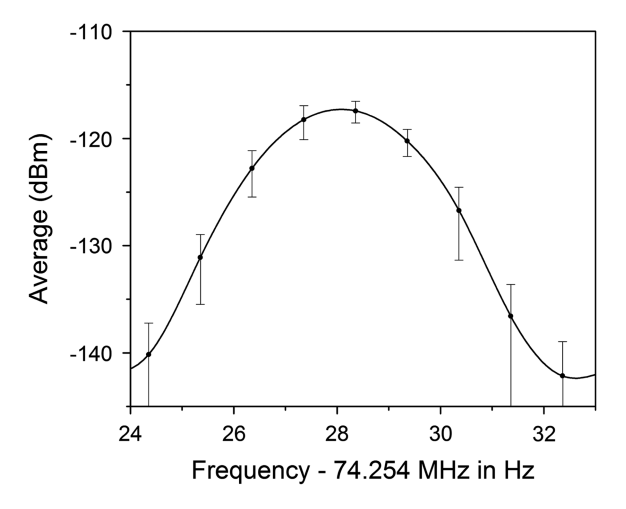


Figure 6. Expanded graph of the mean power at the first harmonic for 24 consecutive scans with an n-type GaN sample in the scanning tunneling microscope, with error bars.

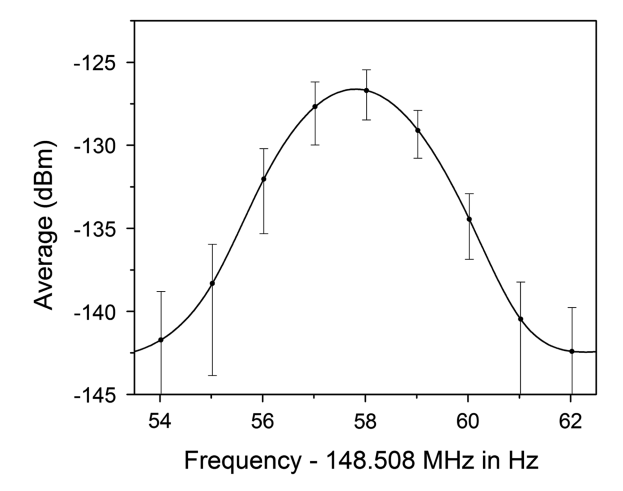


Figure 7. Expanded graph of the mean power at the second harmonic for 24 consecutive scans with an n-type GaN sample in the scanning tunneling microscope, with error bars.

In these figures, the frequency is offset to make the values on the abscissa readable (i.e., 20 Hz is added to 74.254 MHz, etc.). Figures 4 and 6 show the power at the fundamental frequency and Figures 5 and 7 are for the second harmonic. Figures 6 and 7 are expanded and error bars are added to enable interpretation. In each case, the semiconductor had a bias of -9 V relative to the tip for a forward-biased tunneling junction. The DC tunneling current was $1\,\mu\text{A}$, the resolution bandwidth was 2 Hz, and the laser had an average power of 60 mW. The error bars correspond to the mean plus or minus 1 SD, based on the 24 consecutive scans. Figures 6 and 7 show that the apparent linewidth is 2.6 Hz at the two harmonics and this value is primarily due to the 2-Hz resolution bandwidth of the spectrum analyzer.

Figures 6 and 7 show that the MFC with an n-type GaN sample has a power at the second harmonic that is 9 dB less than that at the fundamental frequency. However, equation (1) shows that with a metal sample, the power at the second harmonic is 94% of that at the fundamental frequency. Furthermore, with the semiconductor the power at the fundamental frequency is 25 dB less than that with a gold sample, using the same apparatus and settings. These differences may be understood by considering the different phenomena with metal and semiconductor samples. High-frequency currents in the MFC flow on the surface of a metal sample, so it is possible to make measurements with a bias-T in the sample circuit as shown in Figure 1. However, it has already been noted that with a semiconductor, sample minority carriers are injected to create a sub-nanometer spot of surface charge that is neutralized, by dielectric relaxation, as the injected carriers diverge and interact with the converging majority carriers over a distance of $\sim 20 \,\mu\text{m}$.

Whenever current is injected at a small spot on the surface of an object, the "spreading resistance" at that spot is the dominant component of the resistance of any other contact on the object. This effect is seen using a semiconductor sample in an STM (Flores & Garcia, 1984). For a circular

contact with radius a, the spreading resistance is given approximately by $R_{\rm S}=1/4a\sigma$, where σ is the electrical conductivity (Gelmont & Shur, 1993). There is also a spreading capacitance, but its effects may be neglected at the frequencies of the MFC. Scanning spreading resistance microscopy (SSRM) is a means for carrier profiling in semiconductors, which provides a spatial resolution as fine as 1 nm. This method is based on measuring the spreading resistance by inserting heavily doped diamond nanoprobes into the semiconductor (Vandervorst et al., 2014). However, in our measurements, the minority and majority carriers at a sub-nanometer spot, near the tunneling junction, flow through the spreading resistance ($\sim 1~{\rm M}\Omega$), which may be determined because of its strong effect on the attenuation of the measured MFC.

Figure 8 shows an equivalent circuit for determining the power at the harmonics of the MFC for a grounded semiconductor sample in an STM. For the case of a metal sample, the circuit elements between points P_1 and P_2 , which represent the grounded semiconductor, are deleted. Thus, we would have the circuit we have already described with only the constant current source I_n , the shunting capacitance C_s , and the load resistance R_L , to obtain equation (1). However, point P_1 represents the location of the tunneling junction and point P_2 represents the location of the probe. In our measurements, the semiconductor with a thickness of 0.5 mm was in a grounded sample holder. Resistances R_{S1} and R_{S2} are, respectively, the spreading resistance at the tunneling junction and at the probe, and they have small physical size. The resistance from P_1 to ground is R_{S1} and the resistance from P_2 to ground is R_{S2} . The resistance from P_1 to P_2 equals $R_{S1} + R_{S2}$. The capacitance C_{12} , which is distributed over the length of the semiconductor from P_1 to P_2 , is that between the upper surface of the semiconductor and ground.

For this equivalent circuit, the microwave power delivered to the load, at a specific harmonic with the angular frequency ω , is given by the following expression:

$$P_{L} = \frac{R_{L}I_{0}^{2}}{\left(2 + \frac{R_{3}}{R_{S1}} - \omega^{2}R_{S1}R_{3}C_{S}C_{12}\right)^{2} + \omega^{2}(R_{S1}C_{S} + R_{3}C_{S} + R_{3}C_{2} + R_{3}C_{2})^{2}}$$
$$\left(\frac{R_{S2}}{R_{2} + R_{L2}}\right)^{2}, \tag{2}$$

where
$$R_3 \equiv R_{S2} + \frac{R_{S2}R_L}{R_{S2}R_I}$$
. (3)

 I_0 is the root-mean-square value of the current from the generator, which represents the constant current source in the tunneling junction. For applications of interest in characterizing the semiconductors, $R_{S1} = 1 \text{ M}\Omega$, $R_{S2} = 1 \text{ k}\Omega$, $R_L = 50 \Omega$, $R_3 = 1 \text{ k}\Omega$, $C_S = 6.4 \text{ pF}$, and $C_{12} = 12 \text{ pF}$. Thus, for frequencies near the first few harmonics, equation (2) may be simplified to obtain the following expression:

$$P_L = \frac{R_L I_0^2}{4 + \omega^2 R_{S1}^2 C_S^2 + \omega^4 R_{S1}^2 R_{S2}^2 C_S^2 C_{12}^2}.$$
 (4)

Figure 9 shows the microwave power as a function of the spreading resistance at the tunneling junction, where P_L was

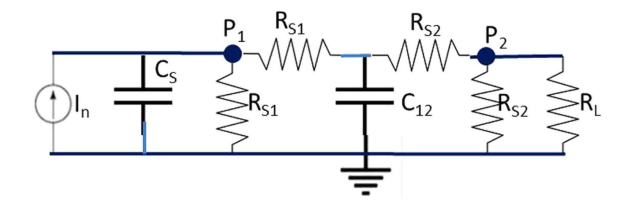


Figure 8. Equivalent circuit for determining the power at harmonics of the microwave frequency comb with a grounded semiconductor sample in a scanning tunneling microscope.

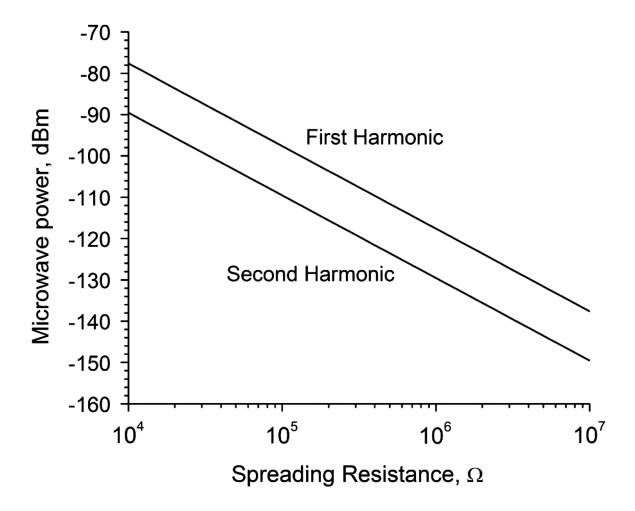


Figure 9. Calculated microwave power versus spreading resistance at the tunneling junction for the first and second harmonics at 74.254 and 148.508 MHz.

calculated using equation (2) for the first and second harmonics at 74.254 and 148.508 MHz, respectively. In these calculations, $R_{S2} = 1 \text{ k}\Omega$, $R_L = 50 \Omega$, $C_S = 6.4 \text{ pF}$, and $C_2 = 12 \text{ pF}$.

Measurements of the MFC with semiconductors require (1) a forward-biased tunneling junction for greater DC tunneling current; (2) a probe making a surface contact within $200\,\mu\text{m}$ of the tunneling junction; (3) using only the first few harmonics, because the higher harmonics roll-off faster than with metal samples; and (4) a mode-locked laser having a photon energy less than the bandgap energy of the semiconductor, to prevent creating electron-hole pairs which cause surge currents that interfere with the measurements.

The NI PXIe-5668R high-performance VSA, with Lab-VIEW programming, enables fast and efficient acquisition, storage, retrieval, and analysis of the data so that every scan was captured and processed. The large data files show occasional sharp changes in the measured microwave power, which we attribute to the feedback mechanism stabilizing the DC tunneling current in the STM. Each time the tip-sample distance is automatically changed to stabilize the tunneling current, this also changes the tip-sample capacitance, which could cause the sharp changes in the measured microwave power. It may be possible to avoid this effect, without disabling the feedback, by switching the spectrum analyzer between the probe and the tip circuit. This would allow direct

determination of the microwave attenuation, instead of only measuring the power that is delivered through the probe.

All of the measurements with gallium nitride were made under ultrahigh vacuum conditions, typically at a working pressure of 2×10^{-9} Torr. However, after the sample was cleaned with HF, it was exposed to the atmosphere for 60 min before the system was pumped. Thus, it is possible that vacuum may not be required for these measurements.

Measurements of the attenuation of the MFC are sensitive to the spreading resistance in a sub-nanometer spot at the tunneling junction, which may enable carrier profiling with sub-nanometer resolution. Roadmaps for the semiconductor industry request that the spatial resolution for carrier profiling be finer than 10% of the dimension at each lithography node. However, this is not possible with present technology at the 7-nm node introduced in 2015, or the 5 and 2-nm nodes that are currently in research mode. SSRM is now the preferred method for high-resolution carrier profiling (Vandervorst et al., 2014), but it changes the lattice at the points where the diamond nanoprobes are inserted (Germanicus et al., 2015). Measurements with an MFC do not require probe insertion and also have the advantage of reduced signal to noise, because of the extremely narrow linewidth, and may determine the dielectric function of the semiconductor as well as the carrier concentration.

Conclusion

Several significant observations can be made by examining Figure 9 and equation (4):

- 1. The quartic term for the frequency in the denominator of equation (4) causes a much faster roll-off in the microwave power at successive frequencies than that measured with metal samples, as shown in equation (1), and this difference is consistent with our measurements with semiconductors.
- 2. Figure 9 shows that a factor of 10 increase in the spreading resistance causes the microwave power to decrease by a factor of 100, which may be understood from the quadratic terms in the denominator of equation (4). Thus, measurements of the attenuation of the MFC are highly sensitive to the spreading resistance at the tunneling junction, which is inversely proportional to the carrier density in a sub-nanometer spot.
- 3. The spreading resistance at the contact of the surface probe with the semiconductor is not critical in these measurements, because it is in series with the spreading resistance at the tunneling junction, which is typically about $1\,\mathrm{M}\Omega$. Thus, it is permissible to use iridium for attaching the probe to the sample, or even a simple pressure contact.

ACKNOWLEDGMENTS

The authors appreciate that National Instruments loaned them a PXI system with an NI PXIe-5668R high-performance

REFERENCES

- Doloca, N.R., Meiners-Hagen, K., Wedde, M., Pollinger, F. & Abou-Zeid, A. (2010). Absolute distance measurement system using a femtosecond laser as a modulator. *Meas Sci Technol* 21, 115302.
- FLORES, F. & GARCIA, N. (1984). Voltage drop in the experiments of scanning tunneling microscopy for Si. *Phys Rev B* **20**, 2289–2291.
- Gelmont, B. & Shur, S. (1993). Spreading resistance of a round ohmic contact. *Solid State Electron* **36**, 143–146.
- Germanicus, R.C., Leclere, P., Guhel, Y., Boudart, B., Touboul, A.D., Deschamps, P., Hug, E. & Eybedn, P. (2015). On the effects of a pressure induced amorphous silicon layer on consecutive spreading resistance microscopy scans of doped silicon. *J Appl Phys* 117, 244306.
- GRAFSTROM, S. (2002). Photoassisted scanning tunneling microscopy. J Appl Phys 91, 1717–1753.
- HAGMANN, M.J., ANDREI, P., PANDEY, S. & NAHATA, A. (2015). Possible applications of scanning frequency comb microscopy for carrier profiling in semiconductors. *J Vac Sci Technol B* **33**, 02B109.

- HAGMANN, M.J., EFIMOV, A., TAYLOR, A.J. & YAROTSKI, D.A. (2011). Microwave frequency-comb generation in a tunneling junction by intermode mixing of ultrafast laser pulses. Appl Phys Lett 99, 011112.
- Hagmann, M.J. & Mousa, M.S. (2007). Simulation of subfemtosecond response in laser-assisted field emission. *Ultramicroscopy* **107**, 849–853.
- Hagmann, M.J., Pandey, S. & Yarotski, D.A. (2012a). Microwave frequency comb attributed to the formation of dipoles at the surface of a semiconductor by a mode-locked ultrafast laser. *Appl Phys Lett* **101**, 231102.
- HAGMANN, M.J., STENGER, F.S. & YAROTSKI, D.A. (2013). Linewidth of the harmonics in a microwave frequency comb generated by focusing a mode-locked ultrafast laser on a tunneling junction. *J Appl Phys* **114**, 223107.
- Hagmann, M.J., Taylor, A.J. & Yarotski, D.A. (2012b). Observation of 200th harmonic with fractional linewidth of 10⁻¹⁰ in a microwave frequency comb generated in a tunneling junction. *Appl Phys Lett* **101**, 241102.
- Lin, M.E., Ma, Z., Huang, F.Y., Fan, Z.F., Allen, L.H. & Morkoc, H. (1994). Low resistance ohmic contacts on wide band-gap GaN. *Appl Phys Lett* **64**, 1003–1005.
- Pollock, C.R., Jennings, D.A., Petersen, F.R., Wells, J.S., Drullinger, R.E., Beaty, E.C. & Evenson, K.M. (1983). Direct frequency measurements of transitions at 520 THz (576 nm) in iodine and 260 THz (1.15 μm) in neon. *Opt Lett* 8, 133–135.
- VANDERVORST, W., SCHULZE, A., KAMBHAM, A.K., MODY, J., GILBERT, M. & EYBEN, P. (2014). Dopant/carrier profiling for 3D-structures. *Phys Status Solidi C* 11, 121–129.
- YASUI, T., YOKOYAMA, S., INABA, H., MINOSHIMA, K., NAGATSUMA, T. & ARAKI, T. (2011). Terahertz frequency metrology based on frequency comb. *IEEE J Sel Top Quantum Electron* 17, 191–201.